An End-to-End Autoencoder-based Non-Orthogonal Multi-Carrier System for Transmission

Yalin Zhou
Dept. of Electronic and Electrical Engineering
University College London
London, United Kingdom
yalin.zhou.23@ucl.ac.uk

Izzat Darwazeh
Dept. of Electronic and Electrical Engineering
University College London
London, United Kingdom
i.darwazeh@ucl.ac.uk

***Abstract*—Multi-carrier techniques remain prime candidates for high-frequency 6G and sub-THz wireless transmission, due their resilience to multi-path effects. Spectrally efficient frequency division multiplexing (SEFDM) conserves bandwidth relative to orthogonal frequency division multiplexing (OFDM) but similarly suffers from high PAPR, which affects the power efficiency of mmWave amplifiers. Moreover, SEFDM suffers from high Inter-carrier Interference (ICI) as a result of bandwidth compression, which limits SEFDM's applications and practical deployment. To ameliorate the effects of these two problems, this work proposes an end-to-end autoencoder-based SEFDM system that generates optimized constellation mapping at the transmitter side for reducing PAPR. at the receiver side, a neural network joint SEFDM detection and demodulation is implemented to remove much of the ICI. Simulation based results show that the proposed autoencoder-based SEFDM system achieves BER, which outperforms linear detection techniques. Furthermore, the results show that our optimized constellation improves the PAPR, in specific threshold regions, when compared to conventional QPSK-mapped OFDM and SEFDM signals.**

***Index Terms*—Autoencoder, OFDM, SEFDM, Deep Learning**

I. Introduction

Multipath effects limit the transmission efficiency of single carrier systems, since the duration of each symbol should ideally be larger than the channel delay spread, which then sets upper bounds at the transmission rate. Multi-carrier systems, which are far more resilient to multipath effects, are the main candidates for high rate systems, including the currently developed 6th generation (6G) systems, aiming to operate from the low GHz to the sub-THz frequency bands. OFDM improves spectrum usage by utilizing orthogonality for overlapping subcarrier, hence it effectively combats multipath interference and frequency-selective fading. OFDM and its variants are currently used in 4G LTE [1] and 5G NR [2].

SEFDM, first proposed in [3], is a multicarrier faster-than-nyquist(FTN) signal [4] with reduced spacing between its subcarriers, to further save bandwidth by factor α ; SEFDM reverts to OFDM when the compression factor $\alpha = 1$. Such bandwidth-saving advantage will be more significant in wide-band transmission scenarios at millimeter wave (mmWave) frequency bands, which means the GHz-level saved bandwidth resource can be allocated for additional data transmission or other emerging applications, such as integrated sensing and communication (ISAC). Experimental work [5], [6] implemented SEFDM in 60-GHz radio over fiber (RoF) transmission and E-band wireless transmission, respectively. Unfortunately, the high peak-to-average power ratio (PAPR) of multi-carrier systems requires power amplifiers with higher dynamic ranges, which leads to low efficiency of power amplifiers and sets limitation on the mmWave hardware in real implementation [7]. Digital pre-distortion techniques such as [8], [9] are proposed to deal with this problem. However, the pre-distortion process is implemented following the digital modulation stage, which inevitably compromises the quality of the signal. Specific techniques for SEFDM PAPR reduction have been studied in [10], but still force system limitations. Another core problem is the inter-carrier interference (ICI) of SEFDM, which requires complex detection methods to be mitigated; such methods have been detailed in [11] and include the use of deep learning as in [12].

The autoencoder is an unsupervised neural network technique with strong nonlinear mapping capabilities; its application in the physical layer has been studied in [13]–[15], where the autoencoder could learn the best constellation mapping, under specific AWGN channels, for better BER performance. In addition, the neural network is also applied for SEFDM detection as discussed in [12], to mitigate nonlinear ICI. Motivated by the strong optimization capability of neural networks, in this paper, an autoencoder-based SEFDM system is designed which reduces the PAPR before the SEFDM modulation process for better use of the power amplifiers in mmWave systems, presenting a deep-learning-driven solution for physical-layer communication. At the transmitter side, one part of this autoencoder outputs the constellation pre-trained with lower PAPR. As such, the reduction of PAPR is carried out in an independent stage, which does not cause distortion and can be combined with a pre-distortion technique to improve performance further. At the receiver, the other part of the autoencoder takes responsibility for SEFDM signal detection *together* with its demodulation to recover the transmitted bits. The loss function for the training process is designed as the combination of target PAPR and lower BER, under specific AWGN channel conditions, by applying different weights. This enhances the practical usability of SEFDM communications by improving the BER performance. The BER performance of this autoencoder-based SEFDM

system outperforms the linear matched receiver FFT and zero-forcing (ZF) detection methods for SEFDM signals [11]. As for the PAPR, when the output constellation of the autoencoder is applied, the PAPR shows an advantage over conventional QPSK-mapped OFDM and SEFDM signals.

II. SEFDM Waveform

SEFDM is a multicarrier signal waveform, which achieves higher spectral efficiency, relative to conventional OFDM, by compressing the spacing between its subcarriers, below the orthogonality limit. Suppose X_n is the complex baseband symbol generated by a constellation mapper with symbol rate R_s, which will be modulated with nth subcarrier, the complex envelope of the baseband modulated SEFDM symbol $z(t)$, with N subcarrier could be expressed as follows,

$$z(t) = \sqrt{\frac{1}{T}} \sum_{n=0}^{N-1} X_n p(t-T) e^{j2\pi\alpha n \Delta f t} \tag{1}$$

where $T = N/R_s$, is the time duration of an SEFDM symbol and $p(t-T)$ represents the pulse shape function. The bandwidth of SEFDM is compressed by a compression factor α, where $\alpha \in (0, 1]$. OFDM can be considered as the case where $\alpha = 1$. The discrete representation of the complex envelope of the SEFDM signal is shown in (2), which is derived by sampling the SEFDM symbols at intervals T/Q where $Q = \rho N$ and the sampling factor $\rho \geq 1$.

$$Z[k] = \sqrt{\frac{1}{Q}} \sum_{n=0}^{N-1} X_n e^{\frac{j2\pi\alpha nk}{Q}} \tag{2}$$

Under ideal channel conditions, the received symbol sequence $\hat{\mathbf{X}} = [\hat{X}_0, \hat{X}_2, \cdots, \hat{X}_{N-1}]$, suffers from ICI, may be linked to te transmitted sequence $\mathbf{X}$ by:

$$\hat{X} = CX \tag{3}$$

where $\mathbf{C}$ is the $N \times N$ correlation matrix, whose elements represent p-row, q-column could be expressed as

$$Cp, q = \frac{1 - e^{j2\pi\alpha(p-q)}}{N(1 - e^{j2\pi\alpha(p-q)/N})} \tag{4}$$

Several generation methods of SEFDM have been explored [16]; for practical systems the low complexity, IFFT-based generation, which is of similar complexity to current OFDM systems, is commonly used and applied in this work, with sampling factor $\rho = 1$. The received symbols $\hat{\mathbf{X}}$, obtained from directly matched FFT demodulation, is the same as (3). In this work, two commonly studied SEFDM detection methods are utlized and contrasted. These are introduced below.

A. Zero Forcing (ZF) Detection

ZF is the simplest of linear detection method that operates by multiplying the received the inverse matrix by $\mathbf{C}$ at the receiver side. For the received and demodulated symbols $\mathbf{R}$, the detected symbols $\hat{\mathbf{X}}_{\text{ZF}}$ could be represents as

$$\hat{X}_{\text{ZF}} = \lfloor C^{-1} R \rceil \tag{5}$$

where $\lfloor \cdot \rceil$ denotes the operation to determine the demodulated symbols by finding the minimum euclidean distance between each possible constellation points.

B. Iterative Detection (ID)

Maximum likelihood is the most powerful of the nonlinear detection technique, but unfortunately it cannot be applied directly in practical systems because of its complexity. Alternative maximum likelihood inspired methods with different search strategies were applied to SEFDM detection, such as in [17]–[20]. Among these, ID [19] is an easy-to-implement and effective detection method, which has already been utilized in experimental work [5]. The constellation points are partitioned into two zones: one comprising points that are less susceptible to decision errors and can be directly determined, while the other consists of points that remain unchanged and proceed to subsequent iterations until the interval of this region is reduced to zero. The iterative process is shown in (6)

$$X_{IDn+1} = R - (C - I) X_{IDn} \tag{6}$$

where I is the $N \times N$ identity matrix. The boundary d of these two zones is defined as $d = 1 - v/t$, where t is the total number of iterations and v is the v^{th} iteration. In this paper, the matched FFT demodulator is followed by either the ZF or ID detection, which are utilized as baselines for comparison with our autoencoder-based SEFDM system.

III. System Design

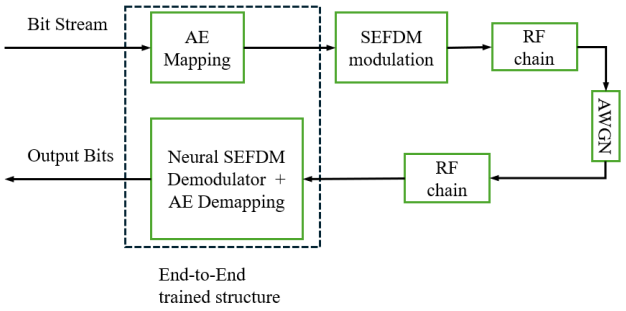

Fig. 1. Simplified block diagram of the trained end-to-end SEFDM communication system.

Fig. 1 shows a simplified block diagram of this newly proposed end-to-end SEFDM system. The bit sequence is first input into the autoencoder mapper to generate the mapped symbols, in a way similar to conventional constellation mapping. This is followed by IFFT based SEFDM modulation. After going through the RF chain, which converts the signal into analogue signal with carriers to be transmitted in the AWGN channel, the signal is received and processed by the RF receiver before being converted into baseband digital signal, which becomes the input into the neural SEFDM demodulator, performing the functions of SEFDM demodulation and detection to recover the received constellation symbols.

Fig. 2 illustrates the working scheme of this end-to-end structure. The transmitter consists of a one-hot encoding layer,

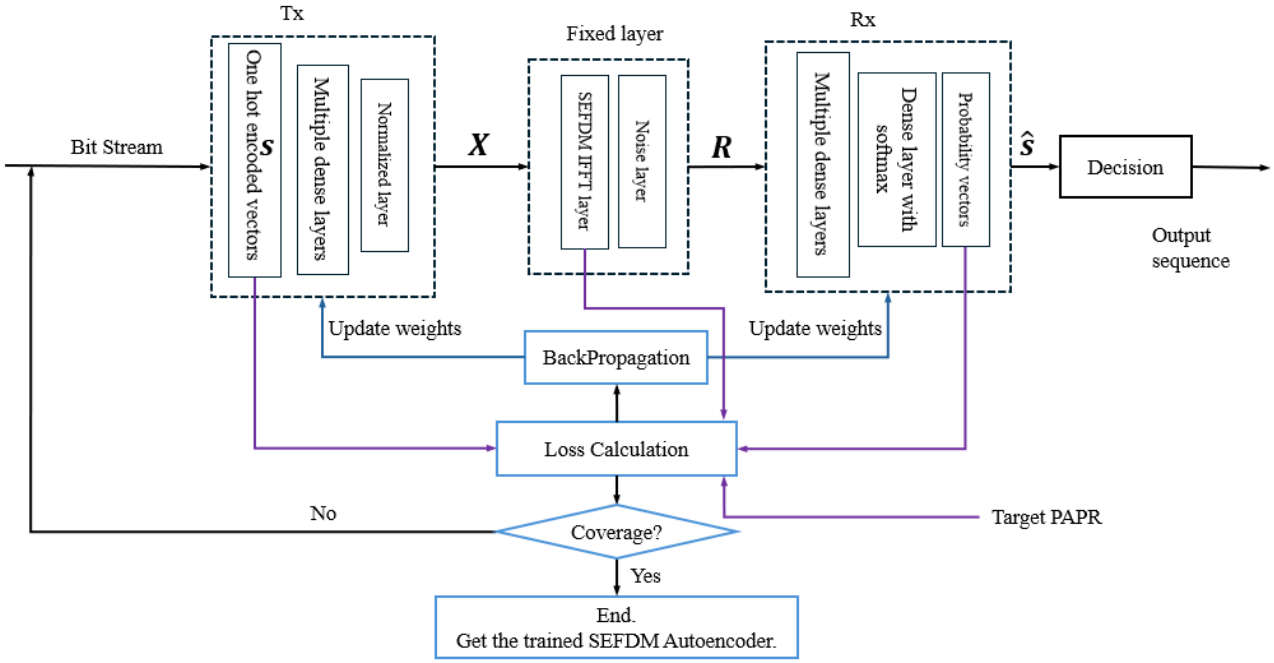

Fig. 2. The structure of the end-to-end autoencoder and training process.

which encodes the input $k \cdot N$ bits into a $N \times 2^k$-dimensional one-hot vector $\mathbf{s}$ and multiple dense layers followed by a normalization layer, where N is the number of subcarriers. The output symbols $\boldsymbol{X}$ of this feedforward neural network is an $N \times M$-dimensional matrix which could be regarded as the learned constellations and is the output of the (k,m) autoencoder, where $\mathbf{k}$ is the size of the binary block to be encoded and $\mathbf{m}$ is the number of output symbols after encoding. The symbols are sent to the fixed layer for SEFDM modulation and AWGN noise addition without undergoing the training process, After the fixed layer, the received SEFDM signal $\boldsymbol{R}$ is obtained and the processed by multiple dense layers and followed by a dense layer with softmax function to obtain the probability vector $\hat{\mathbf{s}}$ which is a $N \times 2^k$-dimensional with same dimension same as $\mathbf{s}$. Then, the gradient is calculated according to the loss function and the weights in neural networks are updated in the backpropagation process. This process is repeated until the loss function coverages, so that the trained end-to-end autoencoder is obtained.

The loss function $\mathfrak{L}$ here is defined in (7) as a weighted linear combination of two loss functions: cross-entropy $\mathfrak{L}_1$ (which measures the discrepancy between the hot encoded vector $\mathbf{s}$ and the output probability vector $\hat{\mathbf{s}}$) and the mean squared error (MSE) $\mathfrak{L}_2$ (which quantifies the difference between the PAPR of the modulated SEFDM signal), with weights λ_1 and λ_2 balancing their contributions.

$$\begin{aligned} \mathfrak{L} &= \lambda_1 \cdot \mathfrak{L}_1 + \lambda_2 \cdot \mathfrak{L}_2 \\ &= -\lambda_1 \cdot \sum_{p=1}^{N} \sum_{i=1}^{M} s_{p,i} \log(\hat{s}_{p,i}) + \\ &\lambda_2 \cdot (PAPR - PAPR_{target})^2 \end{aligned} \tag{7}$$

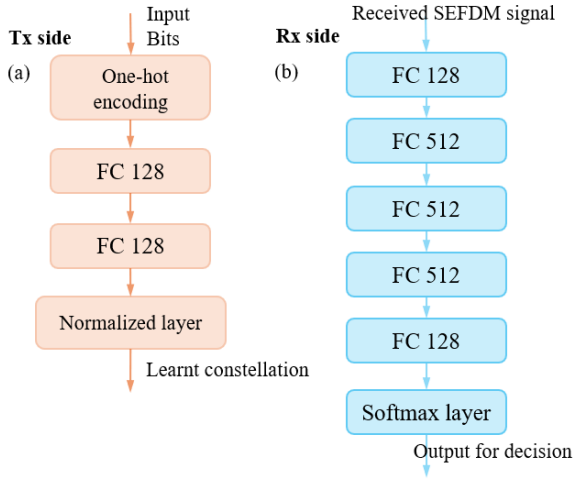

Fig. 3. Neural network implementation with fully connected multiple dense layers (a) at the transmitter and (b) at the receiver.

The calculation of PAPR for discrete signal $z[n]$, sampled at intervals $q \in [0, 1, \cdots, Q-1]$ is expressed in (8)

$$PAPR = \frac{P_{max}}{P_{avg}} = \frac{\max_{q \in [0,1,\cdots,Q-1]} |z[n]|^2}{\frac{1}{Q} \sum_{q=0}^{Q-1} |z[n]|^2} \tag{8}$$

In this paper, λ_1 for cross-entropy loss and λ_2 for MSE are selected as 10 and 10^{-2}, respectively. The weighted linear combination was designed for two main reasons. First, while the PAPR typically has a magnitude around 10 dB, the BER is much lower, ranging from 10^{-5} to 10^{-1}. The weights λ_1 and λ_2 are used to combine them in case the loss function is converged

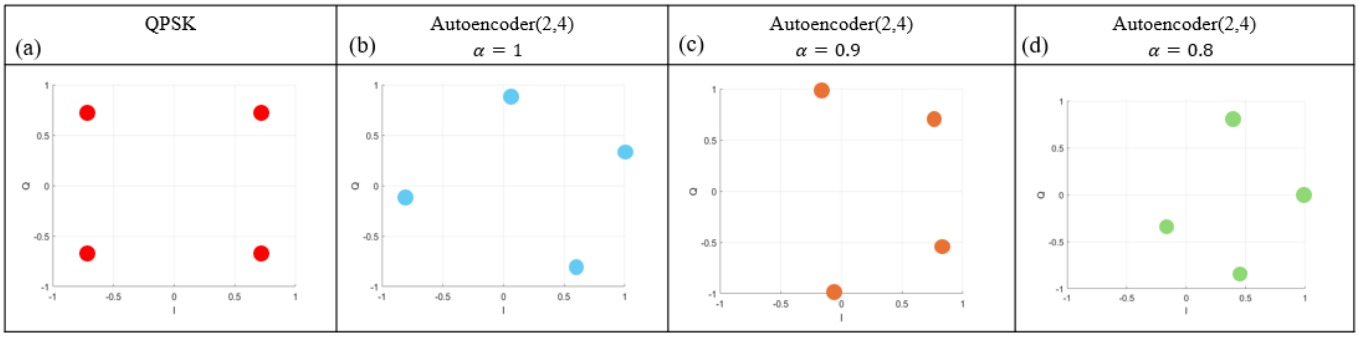

Fig. 4. The mapped symbols obtained by the autoencoder with normalised energy. (a) Conventional QPSK. (b) The constellation output by autoencoder at the transmitter side when $\alpha = 1$. (c) The constellation output by autoencoder at the transmitter side when $\alpha = 0.9$. (d) The constellation output by autoencoder at the transmitter side when $\alpha = 0.8$.

just because the high-level component was optimized; Second, adjusting the value of weights λ_1 and λ_2, the BER and PAPR could be controlled to specific targets in this end-to-end structure which makes itself more flexible.

Fig. 3 shows the design details of neural networks at the transmitter and receiver of the autoencoder-based SEFDM system. At the transmitter, the input bits are first transformed into sparse vectors via one-hot encoding, then passed through two fully connected (FC) layers (each with 128 neurons) for feature extraction and mapping. A normalization step is then applied to obtain the final output constellation mapping scheme. On the receiver side, the received SEFDM signals are fed through five FC layers with neuron sizes shown in Fig. 3b for feature recovery and restoration, and the final symbol classification is obtained via a softmax layer, which generates the possibility of recovered symbols. By jointly optimizing the weights in the neural networks at both the transmitter and receiver, the system adaptively learns the optimal modulation and detection strategy for given channel conditions, thus achieving enhanced robustness and efficiency in the presence of interference and noise. For reliable training, 9.6e4 bits are randomly generated and divided into a training set and a validation set. Specifically, 6.4e4 bits are allocated to the training set, while the remaining 3.2e4 is reserved for validation. These correspond to 4e3 SEFDM symbols in the training set and 2e3 SEFDM symbols in the validation set, ensuring a well-balanced dataset for effective model generalization and performance evaluation. The neural network is trained for 50 epochs using a mini-batch size of 32, with the training data shuffled at the beginning of each epoch to enhance generalization.The optimization process is carried out using the Adam optimizer, which adaptively adjusts the learning rate for each parameter based on first-moment (mean) and second-moment (variance) estimates of the gradients.

IV. Results and Discussion

Fig. 4 illustrates the constellation symbols output by the (2,4) autoencoder at the transmitter side for the same target PAPR and different compression factor α. The absolute distance between some learned constellations becomes smaller compared to the conventional QPSK mapping, which means

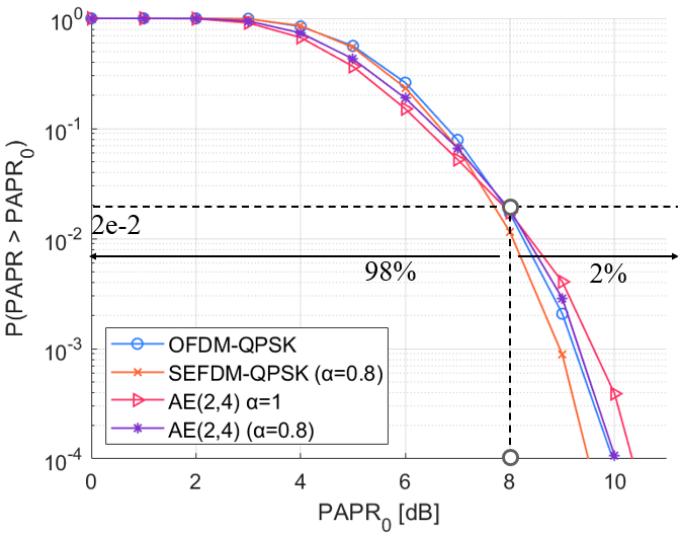

Fig. 5. PAPR comparison of the SEFDM and autoencoder based system.

that the autoencoder system may suffer more from the noise as the trade-off of reducing PAPR.

Fig. 5 shows the complementary cumulative distribution function (CCDF) for the PAPR of the SEFDM signal and the designed (2,4) autoencoder-based SEFDM signal with both compression ratio $\alpha = 0.8$ and subcarrier number $N = 8$, when the target PAPR in the autoencoder training process is set to 5 dB. In most common time ranges (low or medium PAPR thresholds below 8 dB), the CCDF curves corresponding to the autoencoder (pink and purple curves) are consistently lower than those of traditional QPSK-mapped OFDM/SEFDM (blue and orange curves). This indicates that the autoencoder reduces the probability of high peaks more effectively in 98% of all possible SEFDM signals, demonstrating its superiority in peak reduction, which is beneficial for practical applications. However, in the right tail region, where the PAPR threshold exceeds 8 dB, the CCDF curves of conventional OFDM-QPSK and SEFDM-QPSK fall slightly below those of the autoencoder. This suggests that these conventional methods are more effective in suppressing extremely high peaks, making

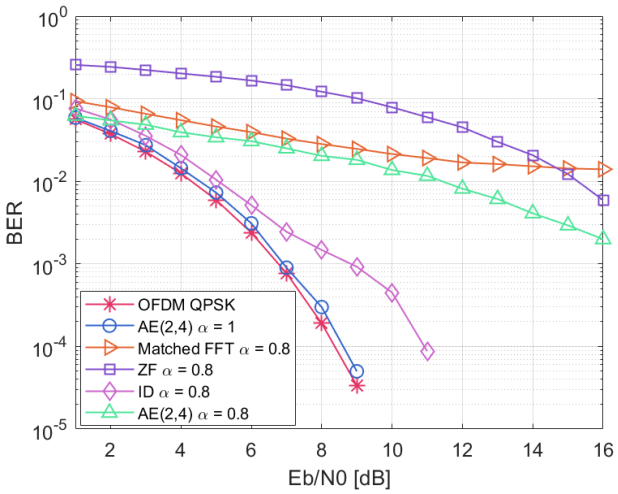

Fig. 6. BER performance of proposed autoencoder-based SEFDM system.

them more suitable for systems that can tolerate high PAPR.

Fig. 6 shows the numerical BER results of the proposed (2,4) autoencoder-based SEFDM system compared with the QPSK-mapped SEFDM signal detected using matched FFT demodulation with/without detection methods with subcarrier N =8. When α = 1, SEFDM becomes OFDM, and the BER performance of the autoencoder-based system is comparable to that of conventional OFDM. When α = 0.8, the autoencoder outperforms matched FFT demodulation with/without ZF detection but remains inferior to ID detection.

V. Conclusions

This paper presents an end-to-end autoencoder designed for SEFDM symbols to improve both the efficiency of power amplifiers in mmWave systems and the error rate performance by directly reducing the PAPR, as an alternative to digital predistortion and by improving the error rate through optimization based on channel conditions. At the transmitter, the proposed architecture generates constellation points through forward propagation, while at the receiver it performs SEFDM signal detection and constellation demapping. The proposed system uses and a joint optimization process through which the training loss function is formulated as a weighted combination of BER and PAPR metrics, ensuring a balance between PAPR reduction and BER performance. Comparative evaluations demonstrate that the proposed method achieves significant PAPR improvements over conventional OFDM/SEFDM systems in the low-to-medium PAPR threshold regions. Furthermore, BER performance analysis shows that beyond reducing the PAPR, our autoencoder-based SEFDM system enhances BER performance, through the autoencoded demodulation and detection processes, and thus outperforms linear ZF detection but remaining less effective than ID detection. Verification of the above results is underway using mmWave laboratory transmission set up over AWGN and realistic propagation channels.

References

[1] *Evolved Universal Terrestrial Radio Access (E-UTRA); Physical Channels and Modulation (Release 16)*, 3rd Generation Partnership Project (3GPP) 3GPP Technical Specification TS 36.211, Jul. 2020.

[2] *NR; Physical Channels and Modulation (Release 17)*, 3rd Generation Partnership Project (3GPP) 3GPP Technical Specification TS 38.211, Jun. 2023.

[3] M. Rodrigues and I. Darwazeh, "A spectrally efficient frequency division multiplexing based communications system," in *Proc. 8th Int. OFDM Workshop*, 2003, pp. 48–49.

[4] J. B. Anderson, F. Rusek, and V. Öwall, "Faster-than-nyquist signaling," *Proceedings of the IEEE*, vol. 101, no. 8, pp. 1817–1830, 2013.

[5] T. Xu, S. Mikroulis, J. E. Mitchell, and I. Darwazeh, "Bandwidth compressed waveform for 60-ghz millimeter-wave radio over fiber experiment," *Journal of Lightwave Technology*, vol. 34, no. 14, pp. 3458–3465, 2016.

[6] H. Ghannam, D. Nopchinda, M. Gavell, H. Zirath, and I. Darwazeh, "Experimental demonstration of spectrally efficient frequency division multiplexing transmissions at e-band," *IEEE Transactions on Microwave Theory and Techniques*, vol. 67, no. 5, pp. 1911–1923, 2019.

[7] W. Jiang, B. Han, M. A. Habibi, and H. D. Schotten, "The road towards 6g: A comprehensive survey," *IEEE Open Journal of the Communications Society*, vol. 2, pp. 334–366, 2021.

[8] D. Morgan, Z. Ma, J. Kim, M. Zierdt, and J. Pastalan, "A generalized memory polynomial model for digital predistortion of rf power amplifiers," *IEEE Transactions on Signal Processing*, vol. 54, no. 10, pp. 3852–3860, 2006.

[9] C. Nader, P. N. Landin, W. Van Moer, N. Björsell, P. Händel, and M. Isaksson, "Peak-to-average power ratio reduction versus digital predistortion in ofdm based systems," in *2011 IEEE MTT-S International Microwave Symposium*, 2011, pp. 1–4.

[10] S. Isam and I. Darwazeh, "Peak to average power ratio reduction in spectrally efficient fdm systems," in *2011 18th International Conference on Telecommunications*, 2011, pp. 363–368.

[11] I. Darwazeh, H. Ghannam, and T. Xu, "The first 15 years of sefdm: A brief survey," in *2018 11th IEEE International Symposium on Communication Systems, Networks Digital Signal Processing (CSNDSP)*, 2018.

[12] T. Xu, T. Xu, and I. Darwazeh, "Deep learning for interference cancellation in non-orthogonal signal based optical communication systems," in *2018 Progress in Electromagnetics Research Symposium (PIERS-Toyama)*, 2018, pp. 241–248.

[13] T. O'Shea and J. Hoydis, "An introduction to deep learning for the physical layer," *IEEE Transactions on Cognitive Communications and Networking*, vol. 3, no. 4, pp. 563–575, 2017.

[14] A. Felix, S. Cammerer, S. Dörner, J. Hoydis, and S. Ten Brink, "Ofdm-autoencoder for end-to-end learning of communications systems," in *2018 IEEE 19th International Workshop on Signal Processing Advances in Wireless Communications (SPAWC)*, 2018, pp. 1–5.

[15] B. Lin, X. Wang, W. Yuan, and N. Wu, "A novel ofdm autoencoder featuring cnn-based channel estimation for internet of vessels," *IEEE Internet of Things Journal*, vol. 7, no. 8, pp. 7601–7611, 2020.

[16] P. N. Whatmough, M. R. Perrett, S. Isam, and I. Darwazeh, "Vlsi architecture for a reconfigurable spectrally efficient fdm baseband transmitter," *IEEE Transactions on Circuits and Systems I: Regular Papers*, vol. 59, no. 5, pp. 1107–1118, 2012.

[17] T. Xu and I. Darwazeh, "Multi-sphere decoding of block segmented sefdm signals with large number of sub-carriers and high modulation order," in *2017 International Conference on Wireless Networks and Mobile Communications (WINCOM)*, 2017, pp. 1–6.

[18] ——, "A soft detector for spectrally efficient systems with non-orthogonal overlapped sub-carriers," *IEEE Communications Letters*, vol. 18, no. 10, pp. 1847–1850, 2014.

[19] T. Xu, R. C. Grammenos, F. Marvasti, and I. Darwazeh, "An improved fixed sphere decoder employing soft decision for the detection of non-orthogonal signals," *IEEE Communications Letters*, vol. 17, no. 10, pp. 1964–1967, 2013.

[20] A. Rashich, A. Kislitsyn, D. Fadeev, and T. Ngoc Nguyen, "Fft-based trellis receiver for sefdm signals," in *2016 IEEE Global Communications Conference (GLOBECOM)*, 2016, pp. 1–6.